Compactons and chaos in strongly nonlinear lattices

Karsten Ahnert and Arkady Pikovsky
Department of Physics and Astronomy, Potsdam University, 14476 Potsdam, Germany
(Received 22 August 2008; revised manuscript received 27 November 2008; published 13 February 2009)

We study localized traveling waves and chaotic states in strongly nonlinear one-dimensional Hamiltonian lattices. We show that the solitary waves are superexponentially localized and present an accurate numerical method allowing one to find them for an arbitrary nonlinearity index. Compactons evolve from rather general initially localized perturbations and collide nearly elastically. Nevertheless, on a long time scale for finite lattices an extensive chaotic state is generally observed. Because of the system's scaling, these dynamical properties are valid for any energy.

DOI: 10.1103/PhysRevE.79.026209 PACS number(s): 05.45.−a, 63.20.Ry

I. INTRODUCTION

Hamiltonian lattices are one of the simplest objects in nonlinear physics. Nevertheless, they still elude full understanding. Already the first attempt to understand nonlinear effects ended with the Fermi-Pasta-Ulam puzzle, which is still not fully resolved (see, e.g., the focus issue on "The "Fermi-Pasta-Ulam" problem—the first 50 years" in [1]); another remarkable feature found only recently is the existence of localized breathers [2]. Quite often nonlinear effects in lattices can be treated perturbatively, leading to well-established concepts of phonon interaction and weak turbulence. Beyond a perturbative account of a weak nonlinearity, one encounters genuine nonlinear phenomena, like solitons and chaos. The level of nonlinearity usually grows with energy, allowing one to follow a transition from linear to nonlinear regimes by pumping more energy in the lattice.

In this paper we study strongly nonlinear Hamiltonian lattices that do not possess linear terms. We restrict our attention to the simplest one-dimensional case where particles interact nonlinearly and no on-site potential is present. We choose the interaction potential in the simplest power form; thus, the lattice is characterized by a single parameter: the nonlinearity index. The equations of motion obey scaling, which means that the dynamical properties are the same for all energies—only the time scale changes. Lattices of this type have attracted a lot of attention recently, in particular due to a prominent example: the Hertz lattice, which describes elastically interacting hard balls: it has nonlinearity index 3/2 [3–6]. We focus our study on the interplay of solitary waves and chaos in such lattices. Some 25 years ago Nesterenko [3,7–9] described a compact traveling-wave solution in the Hertz lattice, which can be understood as a compacton. Compactons have been introduced, in a mathematically rigor form, by Rosenau and Hyman [10,11] for a class of nonlinear partial differential equations (PDEs) with nonlinear dispersion. Compactons can be analytically found if one approximates the lattice equations with nonlinear PDEs, but less is known about the genuine lattice solutions. Below, in Sec. III B we present a numerical procedure for determining traveling waves for an arbitrary nonlinearity index and compare these solutions with those of the approximated PDEs (Sec. III A). Furthermore, we show that compactons naturally appear from localized initial perturbations and relatively robustly survive collisions, but nevertheless evolve to chaos on a long time scale in finite lattices (Sec. IV). The properties of chaos are studied in Sec. V. We demonstrate the extensivity of the chaotic state by calculating the Lyapunov spectrum and study the dependence of the Lyapunov exponents on the nonlinearity index. Some open questions are discussed in the concluding Sec. VI.

II. MODEL

Our basic model is a family of lattice Hamiltonian systems

$$H = \sum_k \frac{p_k^2}{2} + \frac{1}{n+1}|q_{k+1} - q_k|^{n+1}, \tag{1}$$

which are parametrized by one real parameter: the nonlinearity index n. Below we assume that $n \geqslant 1$. The case $n=1$ corresponds to a linear lattice. Another interesting case is $n=3/2$. Such a nonlinearity appears, according to the Hertz law, at the compression in a chain of elastic hard balls. For a realistic system of balls, however, the potential has the form like in (1) only for $q_{k+1}-q_k<0$; for $q_{k+1}-q_k>0$, no attracting force is acting. A simplified realization of such a system is the toy "Newton's cradle", which possesses the same Hertzian interaction law. However, the standard Newton's cradle consists of a few balls (typically 5), which are not enough for the formation of stationary traveling waves. Furthermore, slight intervals between adjacent beads are not excluded, contrary to experiments [4,7] where great care is taken to let the beads be in effective contact. For different aspects of the Hertz chain, see Refs. [6,9,12–21], a review article [22], and references therein. Contrary to this, in our model (1) we assume both repulsive and attracting forces.

Note that the potential in (1) is generally nonsmooth, except for cases $n=1,3,5,\ldots$. Although the dynamics can be easily studied in nonsmooth situations as well, we will mainly focus below on the simplest smooth nontrivial case $n=3$.

The lattice equation of motion reads

$$\ddot{q}_k = |q_{k+1} - q_k|^n \operatorname{sgn}(q_{k+1} - q_k) - |q_k - q_{k-1}|^n \operatorname{sgn}(q_k - q_{k-1}). \tag{2}$$

Since on the right-hand side of (2) only differences enter, it is convenient to introduce the difference coordinates $Q_k = q_{k+1}$

$-q_k$. Then the equations of motion are transformed to

$$\ddot{Q}_k = |Q_{k+1}|^n \operatorname{sgn}(Q_{k+1}) - 2|Q_k|^n \operatorname{sgn}(Q_k) + |Q_{k-1}|^n \operatorname{sgn}(Q_{k-1}). \tag{3}$$

Note that a solitary wave in the variables Q_k corresponds to a kink (shocklike wave) in the variables q_k.

Conservation laws. The equations of motion possess two conservation laws: the energy and the total momentum. The latter can be trivially set to zero by transforming into a moving reference frame.

Scaling. As mentioned in Refs. [3,5,9], the lattice (1) has remarkable scaling properties, due to homogeneity of the interaction energy. It is easy to check that the Hamiltonian can be rescaled according to

$$q = a\tilde{q}, \quad p = a^{(n+1)/2}\tilde{p}, \quad H = a^{n+1}\tilde{H}, \quad t = a^{(1-n)/2}\tilde{t}. \tag{4}$$

Note that this scaling involves only the amplitude and the characteristic time of the solutions: by decreasing the amplitude, one obtains new solutions having the same spatial structure, but evolving slower. We will see that this property has direct consequences for the properties of traveling waves and of chaos.

III. TRAVELING SOLITARY WAVES

In this section localized traveling waves are investigated, first in a quasicontinuous approximation (QCA) and then via numerical solution of the lattice equations. A mathematically rigor proof of the existence of solitary waves in Hamiltonian lattices of type (1) has been given in Refs. [23,24].

A. Quasicontinuous approximation

Here, we represent the solution of the lattice equations (3) as a function of two continuous variables $Q(x,t)$. We are seeking for solitary waves which do not change their sign. For definiteness, we consider $Q \geqslant 0$ (this consideration is therefore suitable for lattices where the nonlinearity index is different for positive and negative displacements Q—e.g., for the Hertz lattice of elastic balls). We present two approaches to find a continuous version of the lattice. In the first one, we approximate the differences between two displacements Q, while in the second one the displacement q at each lattice site is expanded directly.

1. Expansion of differences

Here we look for a direct quasicontinuous approximation of Eq. (3). Expanding the difference coordinates Q_k up to fourth order, we obtain

$$Q^n_{k\pm1} \approx Q^n(x,t) \pm h[Q^n(x,t)]_x + \frac{h^2}{2}[Q^n(x,t)]_{xx} \pm \frac{h^3}{6}[Q^n(x,t)]_{xxx} + \frac{h^4}{24}[Q^n(x,t)]_{xxxx}, \tag{5}$$

where h is the spatial difference between two lattice sites and the subscripts denote differentiation with respect to x. Inserting (5) into (3) and setting $h=1$, one arrives at the partial differential equation

$$[Q(x,t)]_{tt} = [Q^n(x,t)]_{xx} + \frac{1}{12}[Q^n(x,t)]_{xxxx}. \tag{6}$$

Equation (6) belongs to a class of strongly nonlinear PDEs, because the dispersion term with the fourth derivative is nonlinear. The equation does not possess linear wave solutions (this situation has been called "sonic vacuum" by Nesterenko[3]), but it has nontrivial nonlinear ones. In this way it is very similar to a family of strongly nonlinear generalizations of the Korteveg–de Vries equation, studied in [10], and can be considered as a strongly nonlinear version of the Boussinesq equation (11).

Now we seek traveling-wave solutions of (6) by virtue of the ansatz

$$Q(x,t) = Q(x - \lambda t) = Q(s). \tag{7}$$

Then (7) reduces to the ordinary differential equation (ODE)

$$\lambda^2 Q_{ss} = [Q^n]_{ss} + \frac{1}{12}[Q^n]_{ssss}. \tag{8}$$

Furthermore, we assume that the solution tends to zero as $s \to \pm\infty$. Thus after integrating twice we obtain

$$\lambda^2 Q = Q^n + \frac{1}{12}[Q^n]_{ss}. \tag{9}$$

This equation also appears in the traveling-wave ansatz for the $K(n,n)$ equation in [10]. Equation (9) can be solved for an arbitrary power n by

$$Q(s) = |\lambda|^m A_1 \cos^m(B_1 s), \tag{10a}$$

with

$$m = \frac{2}{n-1}, \quad A_1 = \left(\frac{n+1}{2n}\right)^{1/(1-n)}, \quad B_1 = \sqrt{3}\frac{n-1}{n}. \tag{10b}$$

2. Expansion of displacements

Another type of quasi continuum can be obtained if we approximate Eq. (2). Now the displacement q at each lattice site is written as a continuous variable, which for the same order of the spatial derivative as in (5) gives

$$q_{k\pm1} = q \pm hq_x + \frac{h^2}{2}q_{xx} \pm \frac{h^3}{6}q_{xxx} + \frac{h^4}{24}q_{xxxx}. \tag{11}$$

Inserting this expansion into the equations of motion (2) and collecting all terms up to order of h^{n+3} yields

$$[q]_{tt} = h^{n+1}[q_x^n]_x + \frac{h^{n+3}}{12}\left([q_x^n]_{xxx} - \frac{n(n-1)}{2}[q_x^{n-2}q_{xx}^2]_x\right). \tag{12}$$

This equation is the long-wave approximation of Nesterenko [3,9]. To compare it with Eq. (6), we differentiate (12) with respect to x, define $\tilde{Q}=hq_x$, and set $h=1$:

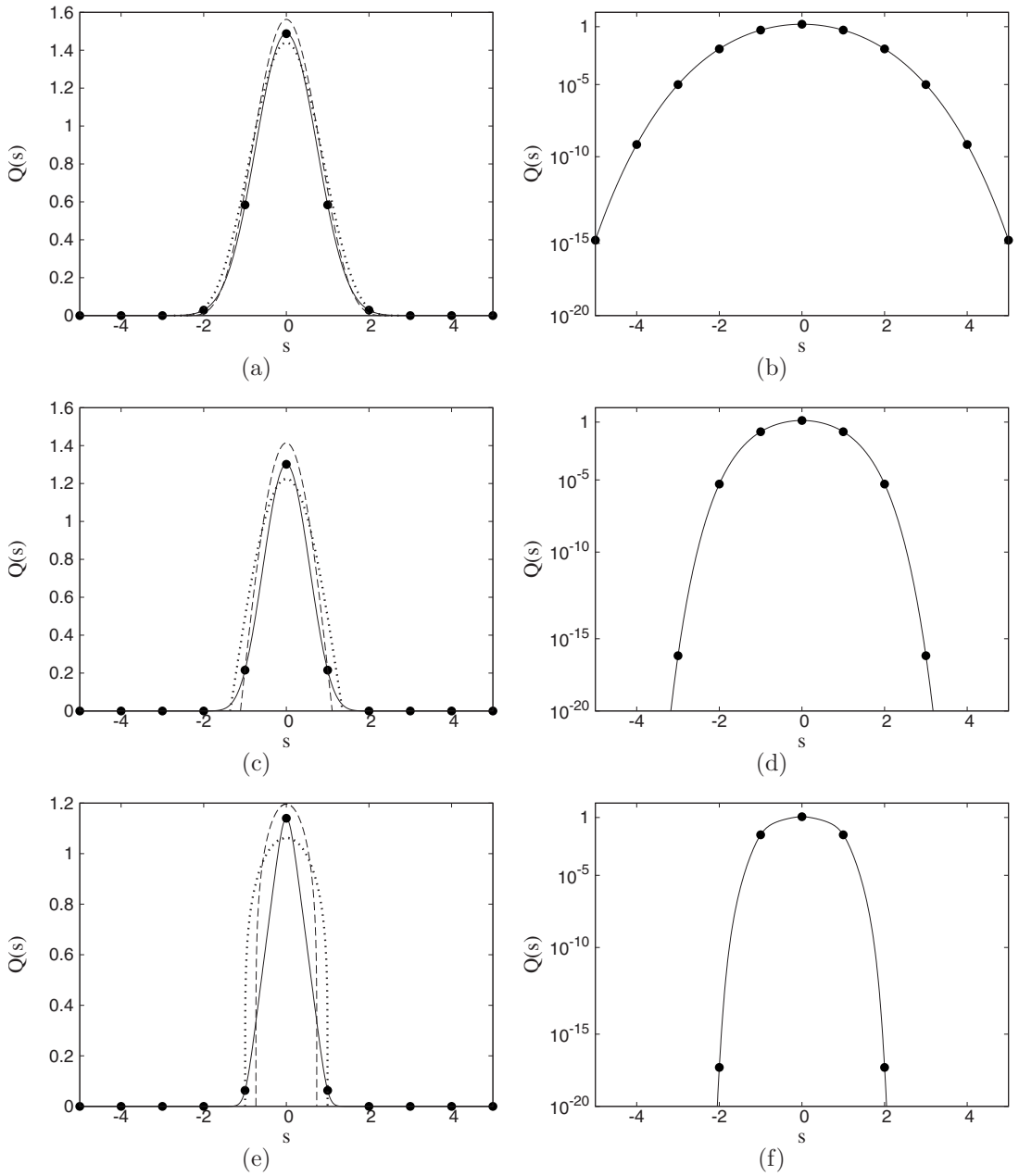

FIG. 1. The traveling waves obtained from (19a) and (19b) for various powers n. Markers show the wave on the lattice, dotted lines show the corresponding solutions of the quasicontinuous approximation (6), and dashed lines show solutions of the QCA (13). Left column: normal scale. Right column: logarithmic scale. (a), (b) $n=3/2$; (c), (d) $n=3$; (e), (f) $n=11$. Note that the width w of the compacton decreases as n increases.

$$[\tilde{Q}]_{tt} = [\tilde{Q}^n]_{xx} + \frac{1}{12}\left([\tilde{Q}^n]_{xxxx} - \frac{n(n-1)}{2}[\tilde{Q}^{n-2}\tilde{Q}_x^2]_{xx}\right). \quad (13)$$

One can see that there is an additional term in (13) compared to (6). This is not so much surprising, as these two quasicontinuous approximations correspond to expansions at the different positions of the original lattice; this effect is well known for approximations of Hamiltonian lattices with PDEs [25]. Because in the problem we do not have a small parameter (the lattice spacing $h=1$ is not small compared to the wavelength), none of the equations (6) and (13) can be expected to be exact in some asymptotic sense. Instead, one has to justify them by comparing the solutions with those of the full lattice problem; see Sec. III B below.

To find traveling waves in the direct expansion, we use again the ansatz (7), $\tilde{Q}(x,t)=\tilde{Q}(x-\lambda t)=\tilde{Q}(s)$. Inserting this ansatz and integrating twice yields then, analogous to (9),

$$\lambda^2\tilde{Q} = \tilde{Q}^n + \frac{1}{12}[\tilde{Q}^n]_{ss} - \frac{n(n-1)}{24}\tilde{Q}^{n-2}\tilde{Q}_s^2. \quad (14)$$

One partial solution of this ordinary differential equation can also be written as

$$\tilde{Q}(s) = |\lambda|^m A_2 \cos^m(B_2 s), \tag{15a}$$

but with different constants A_2 and B_2 (cf. [19,26]):

$$m = \frac{2}{n-1}, \quad A_2 = \left(\frac{2}{1+n}\right)^{1/(1-n)}, \quad B_2 = \sqrt{6\frac{(n-1)^2}{n(n+1)}}. \tag{15b}$$

The solutions (10a), (10b), (15a), and (15b) do not satisfy boundary conditions. Moreover, they intersect with another, trivial solution of (8), $Q=0$. Remarkably, because of the degeneracy of Eqs. (8) and (14) at zero, one can merge the periodic solutions (10a), (10b), (15a), and (15b) with the trivial solution $Q=0$ (see a detailed discussion in [10,11]):

$$Q(s) = \begin{cases} |\lambda|^m A_i \cos^m(B_i s), & |s| < \dfrac{\pi}{2B_i}, \\ 0, \quad \text{otherwise}, \end{cases} \tag{16}$$

with $i=1,2$. This gives a compacton—a solitary wave with a compact support—according to definition [10,11]. For other, nonsolitary solutions of (13), see, e.g., [9,26]. Note that due to the symmetries $x \to -x$ and $Q \to -Q$, solitary waves with both signs of velocity λ and of amplitude A are the solutions.

It is important to check the validity of the solution (16) by substituting it back to (8) or (13). Then no terms are singular for the case $m>2$ only—i.e., for $n<2$. Thus, the constructed compacton solution (16) is, strictly speaking, not valid for strong nonlinearities $n \geqslant 2$. This conclusion is, however, only of small relevance for the original lattice problem. Indeed, the PDE (6) or (12) is only an approximation of the lattice problem: because the spatial extent of the solution (16) is finite, there is no small parameter allowing us to break expansion (5) or (11) somewhere. Just breaking it after the fourth derivative is arbitrary and can be justified only by the fact that in this approximation one indeed finds reasonable solutions at least for some values of n. A real justification can come only from a comparison with the solutions of the lattice equations, to be discussed in the next subsection. And there we will see that the solution can be found both for weak and strong nonlinearities $n>2$.

B. Traveling waves in the lattice

In the lattice, the traveling-wave ansatz reads $Q_k(t)=Q(k-\lambda t)=Q(s)$. Inserting this ansatz into the lattice equations (3) yields

$$\lambda^2 Q''(s) = Q^n(s-1) - 2Q^n(s) + Q^n(s+1). \tag{17}$$

We employ now the scaling (4) and set $\lambda=1$. As demonstrated in [27], this advanced-delay differential equation can be equivalently written as an integral equation

$$Q(s) = \int_{s-1}^{s+1} (1-|s-\xi|) Q^n(\xi) d\xi. \tag{18}$$

[One can easily check the equivalence by differentiating (18) twice.] We can now, following the approach of Petviashvili [28,29], construct an iterative numerical scheme to solve the integral equation (18). Starting with some initial guess Q_0, one constructs the next iteration via

$$Q_{i+1} = \left(\frac{\|Q_i\|}{\|Q_*\|}\right)^{\alpha} Q_* \tag{19a}$$

and

$$Q_* = \int_{s-1}^{s+1} (1-|s-\xi|) Q_i^n(\xi) d\xi \tag{19b}$$

(practically, we used the L_1 norm for $\|\cdot\|$). We have used $\alpha = \frac{n}{n-1}$, which ensured convergence of the iterative scheme. The integral in (19a) and (19b) was numerically approximated by virtue of a fourth-order Lagrangian integration scheme [30]. In Fig. 1 the traveling waves for various powers n are shown. Using the logarithmic scale, one clearly recognizes the compact nature of the waves.

In Fig. 2 we show the dependences of the total energy E, the solution L_1 norm N_{L_1} and the amplitude Q_{max} of the found waves on the nonlinearity index n for a fixed wave velocity of $\lambda=1$. Remarkably, the effective width N_{L_1}/Q_{max} decreases with increasing nonlinearity index and it seems that the profile of the compacton converges to a triangular shape as $n \to \infty$. A similar result has been obtained in [20], where the dependence of the pulse velocity on the nonlinearity index has been analyzed for large n in the binary collision approximation.

C. Estimation of the tails

It is clear from the integral form (18) that the solution cannot have a compact support. In this section we estimate the decay of the tails. We start with (18) and substitute $Q(s)=e^{-f(s)}$:

$$Q(s) = \int_{s-1}^{s+1} (1-|s-\xi|) e^{-nf(\xi)} d\xi. \tag{20}$$

We consider the tail for large $s>0$ if we assume a rapid decay of $Q(s)$; then, the integrand in (20) has a sharp maximum at $s-1$. Thus we can approximate the integral using the

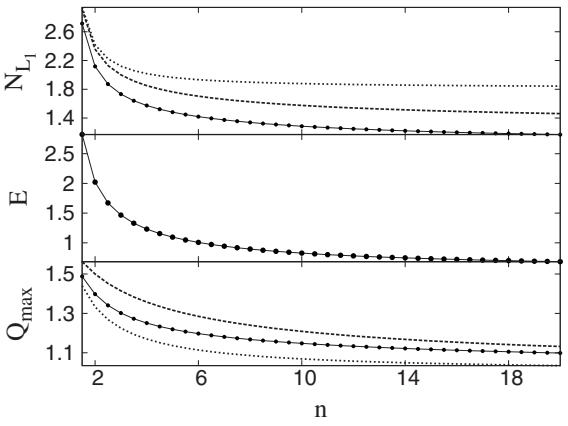

FIG. 2. The dependence of the amplitude Q_{max}, the energy E, and the L_1 norm N_{L_1} of a compacton on the nonlinearity index n. In this plot $\lambda=1$. For comparison, the curves from the quasicontinuous approximation are shown with dotted lines for the Eq. (6) and with dashed lines for Eq. (13).

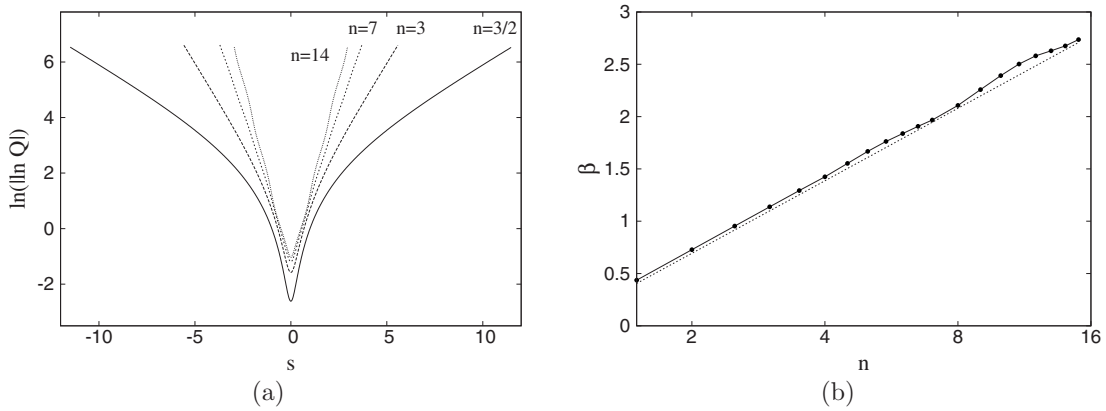

FIG. 3. (a) The tails of the compactons in double-logarithmic scale. (b) Comparison of the estimate (27) with the compactons obtained from (19a) and (19b).

Laplace method. At the maximum we expand $f(\xi)$ into a Taylor series around $s-1$, keeping only the leading first-order term:

$$Q(s) \approx \int_{s-1}^{s+1} (1-|s-\xi|)\exp\{-nf(s-1)-nf'(s-1) \times[\xi-(s-1)]\}d\xi. \quad (21)$$

We shift the integration range

$$Q(s) \approx e^{-nf(s-1)} \int_0^2 \xi e^{-nf'(s-1)\xi} d\xi, \quad (22)$$

where we also replace the decreasing part of the kernel with ξ. Since this integrand decreases very fast, we can set the upper bound of the integration to infinity; then, by partial integration we obtain

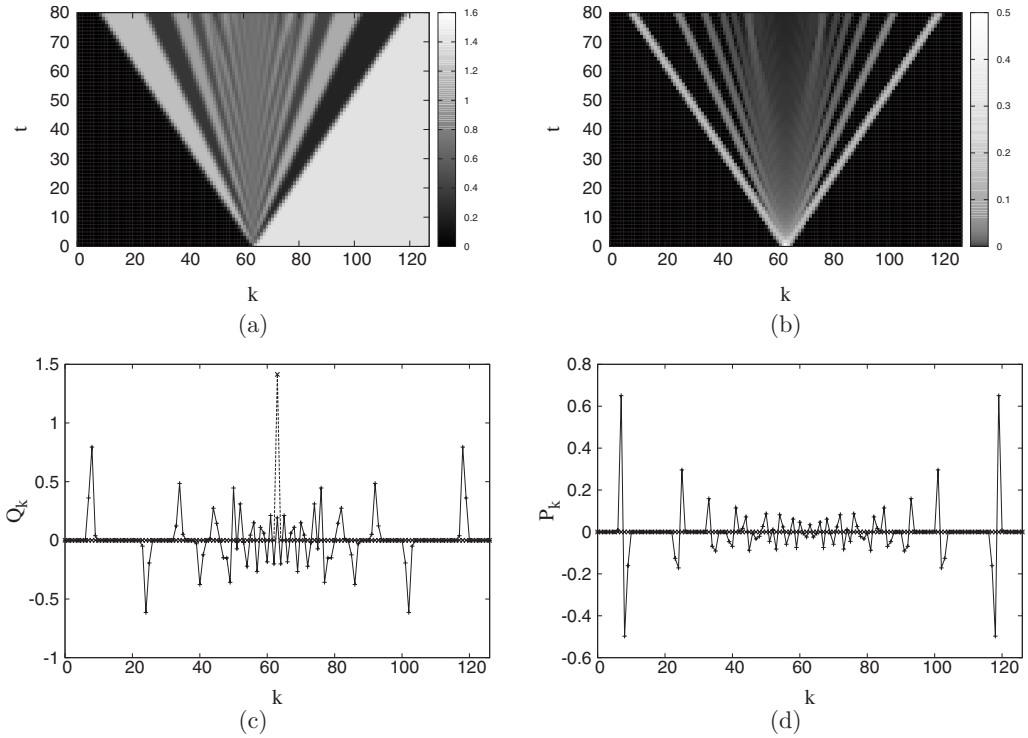

FIG. 4. Evolution from an initial step for the nonlinearity index $n=3$. The lattice length is $N=128$, and open boundary conditions [hence $\ddot{q}_1=(q_2-q_1)^n$ and $\ddot{q}_N=-(q_N-q_{N-1})^n$] are used. The initial conditions are $q_k(t=0)=(n+1)^{1/(n+1)}$ for $k>64$ and 0 otherwise; initial momenta are zero. Different plots show different quantities of the lattice: (a) the coordinates q_k, (b) the energy $\mathcal{E}_k$ defined in (28), (c) the difference coordinates $Q_k=q_{k+1}-q_k$ at time $t=80$ (the initial state at $t=0$ is shown here as the dashed line), and (d) the difference momenta $P_k=p_{k+1}-p_k$ at $t=80$. The compactons originating from this initial state are clearly separated near the borders of the chain; those in the middle part are still overlapped.

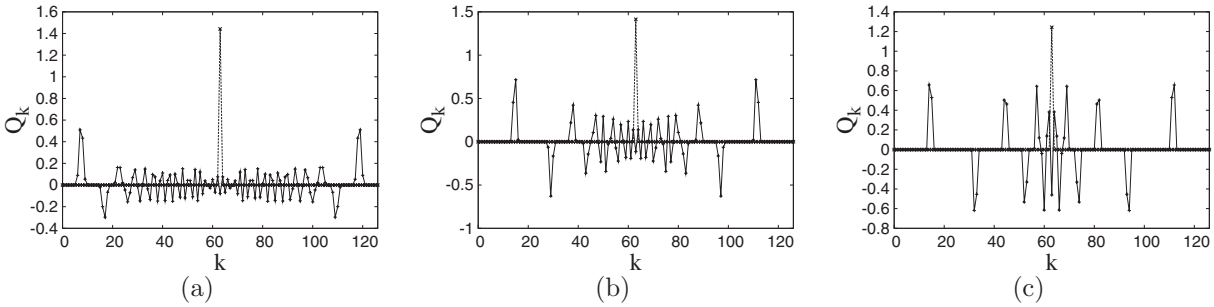

FIG. 5. Evolution of an initial step (like in Fig. 4) for various nonlinearity indices (a) $n=1.5$, (b) $n=3$, and (c) $n=10$. The initial state is shown as a dashed line; the solid line is the state at time $t=80$.

$$Q(s) = e^{-f(s)} \approx \frac{e^{-nf(s-1)}}{[nf'(s-1)]^2}. \tag{23}$$

Taking the logarithm of this equation yields

$$-f(s) = -nf(s-1) - 2\ln[nf'(s-1)]. \tag{24}$$

Since we expect that $f(s)$ is a rapidly growing function of s, we can neglect the logarithmic term and obtain

$$f(s) = nf(s-1). \tag{25}$$

This equation is solved by

$$f(s) = Cn^s = Ce^{\ln(n)s}, \tag{26}$$

where C is an arbitrary constant. Finally we obtain that the tail decays superexponentially:

$$Q(s) = e^{-f(s)} \approx e^{-Cn^s} = \exp\{-C\exp[\ln(n)s]\}. \tag{27}$$

This expression was first obtained by Chatterjee [5] using a direct expansion of the advanced-delayed equation (17).

In Fig. 3(a) we show the tails of the compactons for various values of n, and in Fig. 3(b) we compare the estimated decay rate (27) with compactons obtained numerically from the traveling-wave scheme (19a) and (19b). To obtain the double-logarithmic decay rate $\beta = d\ln\{|\ln[Q(s)]|\}/ds$, we first compute $\ln\{|\ln[Q(s)]|\}$ and then the derivate is calculated using a spline smoothing scheme [31]. To suppress small oscillations of the tails, we average the numerical obtained derivative in the last $1/6$ of the compacton domain. The numerical value of β is shown in Fig. 3(b). Both coincide very well.

IV. EVOLUTION AND COLLISIONS OF COMPACTONS

A. Appearance of compactons from localized initial conditions

The compact solitary waves constructed in the previous section are of relevance only if they evolve from rather general, physically realizable initial conditions. For an experimental significance (see [4,7] for experiments with Hertz beads), it is furthermore important that the emerging compact waves be established on relatively short distances; otherwise, dissipation (which has not been considered here) will suppress their formation. We illustrate this in Figs. 4 and 5. There we report on a numerical solution of the lattice equations (2) on a finite lattice of length $N=128$ [so that at the boundaries $\ddot{q}_1 = |q_2 - q_1|^n \mathrm{sgn}(q_2 - q_1)$ and $\ddot{q}_N = -|q_N - q_{N-1}|^n \mathrm{sgn}(q_N - q_{N-1})$ hold]. One of the quantities we report is the local energy at site k defined as

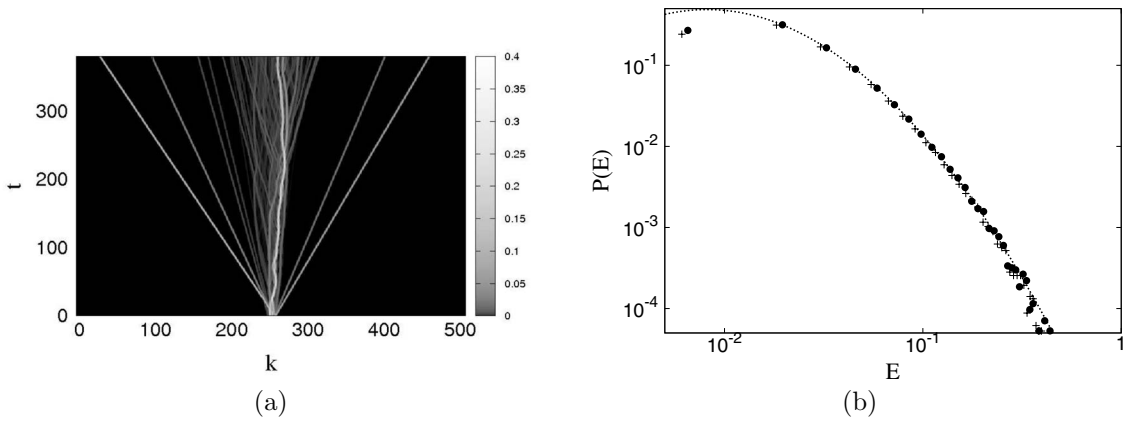

FIG. 6. (a) Compactons emerging from localized random initial conditions. The nonlinearity index is $n=3$. The gray scale corresponds to the energy (28) of the lattice site. (b) Energy distribution of the compactons emitted from localized random initial conditions. The statistics was obtained from 60 000 simulations; in each simulation, the lattice was integrated to the time $T=1000$ and the energy distributions of the compactons emerging to the right (black circles) and left (crosses) have been determined. The distributions obey in very good approximation $P(E) \sim E^{-a\ln(E)-b}$, with $a=0.57$ and $b=5.47$.

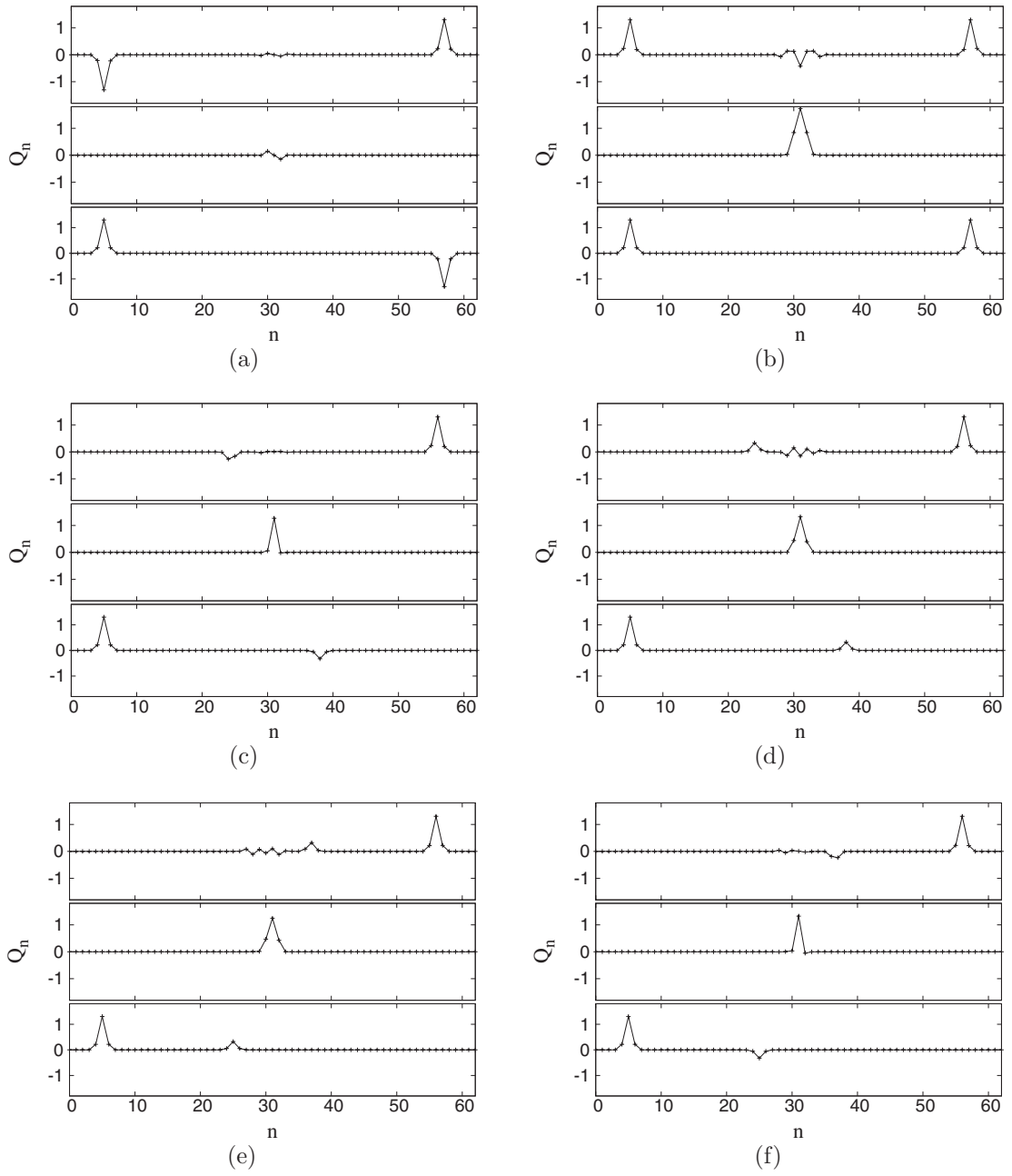

FIG. 7. Collisions of compactons in the Hamiltonian lattice with $n=3$. Shown are difference coordinates Q_k. We have considered six different collision scenarios. In each plot the lower panel is the initial configuration of the lattice, the middle panel is the state of the lattice at some time during the maximal overlap, and the upper panel shows the lattice past the collision. (a) Compactons of equal energy having opposite amplitudes and velocities, (b) compactons of equal energies and amplitudes but opposite velocities, (c) compactons of different energies having amplitudes and velocities of opposite signs, (d) compactons of different energies having amplitudes of the same and velocities of opposite signs, (e) compactons of different energies having velocities and amplitudes of the same sign, and (f) compactons of different energies having velocities of the same sign and amplitudes of opposite signs.

$$\mathcal{E}_k = \frac{p_k^2}{2} + \frac{1}{2(n+1)}(|q_{k+1} - q_k|^{n+1} + |q_k - q_{k-1}|^{n+1}). \quad (28)$$

As an initial condition, we have chosen a kink in the variables q_k: $q_k=(n+1)^{1/(n+1)}$ for $k>64$ and $q_k=0$ elsewhere. This profile has unit energy; it corresponds to the localized initial condition in the variable Q: $Q_k=\delta_{k,64}(n+1)^{1/(n+1)}$. The evolution of different variables is shown in Fig. 4. From the initial pulse of Q, a series of compactons with alternating signs is emitted in both directions. The amplitude of the perturbation near the initially seeded site decreases and correspondingly increases a characteristic time of the evolution. We expect that at large times, compactons with small amplitudes will continue to detach. In Fig. 5 we show the evolution from the initial step for different nonlinearities $n=1.5, 3, 10$. The plots look very similar, and compactons are

emitted in every case. The number of emitted compactons and their amplitudes depend on the nonlinearity index.

In our next numerical experiment, we studied the emergence of compactons not from a sharp step in the coordinates q_k, but from localized random initial conditions. In Fig. 6(a) we show a typical evolution in a lattice of length $N=512$ (with nonlinearity index $n=3$) resulting from random initial conditions q_k in the small region $N/2-5 \leqslant k < N/2+5$ around the center of the lattice. In this region the coordinates q_k have been chosen as independent random numbers, identically and symmetrically uniformly distributed around zero, while $p_k(0)=0$. Furthermore, the energy of the lattice was set to $E=1$ by rescaling. In a particular realization of Fig. 6(a), at the initial state two compactons emerge to the right and four compactons to the left. In the center of the lattice, a chaotic region is established and slowly spreads over the lattice, possibly emitting more compactons on a longer time scale. In Fig. 6(b) we perform a statistical analysis of this setup by showing the energy distribution of compactons emitted from localized random initial conditions as described above. This distribution was obtained from 60 000 simulations; in each simulation, the energy of the emitted compactons has been determined and counted. The functional form of the distribution obeys in very good approximation $P(E) \sim E^{-a \ln(E)-b}$, with $a=0.57$ and $b=5.47$.

B. Collisions of compactons

As we have demonstrated above, compactons naturally appear from rather general initial conditions. To characterize their stability during the evolution, we study their stability to the collisions. This study is not complete, but only illustrative, as in Fig. 7, we exemplify different cases of collision of two compactons in a lattice with $n=3$. These six setups present all possible scenarios of two compactons: (i) two colliding compactons with the same amplitudes, (ii) two compactons with different amplitudes moving toward each other, and (iii) two compactons with different amplitudes moving in the same direction and passing each other. Each of these three cases has two subcases, because the amplitudes can have the same or different sign. It should be mentioned that these six collisions do not represent the complete picture of all collisions. Moreover, we have not varied parameters such as the distance between two colliding compactons or their amplitudes.

In all the cases presented, the initial compactons survive the collision: they are not destroyed, although they do not survive the collision unchanged. In all cases the collision is nonelastic; some small perturbations (which presumably on a very long time scale may evolve into small-amplitude compactons) appear.

Because of this nonelasticity, on a finite lattice after multiple collisions initial compactons get destroyed and a chaotic state appears in the lattice, as illustrated in Fig. 8. There we show the evolution of the two compactons with the same amplitude and sign of the amplitude for three different nonlinearities: $n=3$, $n=9/2$, and $n=11$. In the first two cases, the chaotic state establishes relatively fast. In the third simulation with $n=11$, the situation is different. Here the chaotic state does not appear even on a very long time scale. We run the simulation for very long times up to $T=2\times10^5$, but could not observe the development of a chaotic state. We have checked this phenomenon also for higher values of n with the same result. Presumably, these initial conditions lie on a stable quasiperiodic orbit or are extremely close to such a one.

V. CHAOS IN A FINITE LATTICE

As demonstrated above, in a finite lattice general initial conditions evolve into a chaotic state. For characterization of chaos, we use Lyapunov exponents. The chaotic state of the lattice has also been characterized in [22,32] by the means of the velocity distribution of the lattice site. It has been found that the lattice possesses a quasinonequilibrium phase, characterized by a Boltzmann-like velocity distribution, but without energy equipartition.

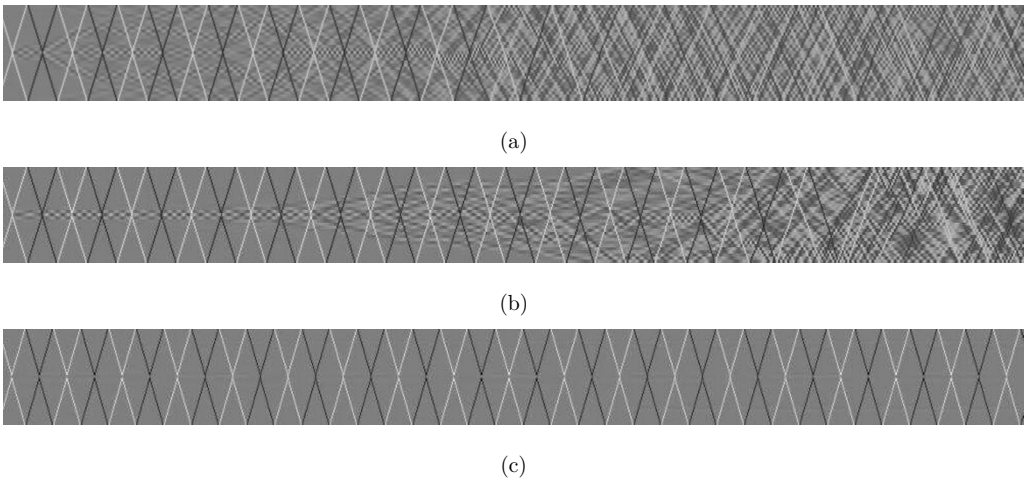

FIG. 8. Collisions of compactons and emergence of chaos after multiple collisions. Different plots show different nonlinearity indices (a) $n=3$, (b) $n=9/2$, and (c) $n=11$. Time increases from left to right, and the difference coordinates Q_k are shown in gray scale. Remarkably the elasticity of the collision increases with increasing nonlinearity index n, so that practically no irregularity appears at $n>10$.

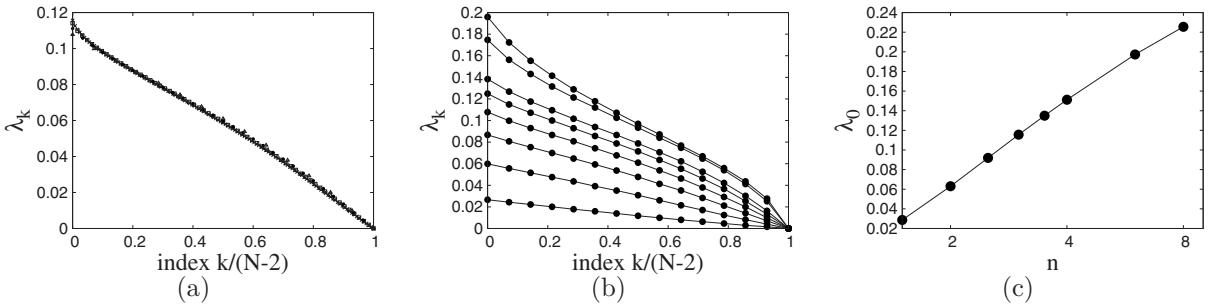

FIG. 9. Lyapunov exponents of the Hamiltonian (1). (a) The Lyapunov spectra for one fixed nonlinearity index $n=3$ and different values of lattice length $N=16,32,64,128$. The index axis is normalized to 1. (b) The Lyapunov spectra λ_j for various values of the nonlinearity index n (from bottom to top, $n=1.5,2,2.5,3,3.5,4,6,8$) and fixed lattice length $N=16$. Larger values of n produce stronger chaos than smaller ones. (c) The largest Lyapunov exponent λ_1 for different values of n. The horizontal axis is logarithmic, thus, one can see that roughly $\lambda_0 \sim \text{const} \times \ln(n)$.

First, we check that chaos in the lattice is extensive; i.e., the Lyapunov exponents form a spectrum when the system size becomes large [Fig. 9(a)]. This property allows us to extend the calculations of finite lattices to the thermodynamic limit. Note that due to the two conservation laws, four Lyapunov exponents vanish; we have not found any more vanishing exponents, indicating the absence of further hidden conserved quantities.

For a lattice of length $N=16$, the dependence of the Lyapunov exponents on the nonlinearity is shown in Fig. 9(b). For a fixed total energy (we have set $H=N=16$ in these calculations), the Lyapunov exponents grow with the nonlinearity index. The plot presented in Fig. 9(c) indicates that $\lambda_{\max} \propto \ln n$, although we did not consider very high nonlinearity indices to make a definite conclusion on the asymptotics for large n.

We stress here that because of the scaling of the strongly nonlinear lattices under consideration, chaos is observed for arbitrary small energies—only the Lyapunov exponents decrease accordingly.

VI. CONCLUSION

In this paper we have studied strongly nonlinear Hamiltonian lattices, with a focus on compact traveling waves and on chaos. We have presented an accurate numerical scheme allowing one to find solitary waves. Moreover, from the integral form representation used one easily derives the superexponential form of the tails. In this way we have confirmed this remarkable result by Chatterjee [5] by another analytical method and by accurate numerical analysis. The constructed compactons were then studied via direct numerical simulations of the lattice. Their collisions are nearly elastic, but the small nonelastic components on a long time scale destroy the localized waves and result in a chaotic state. Chaos appears to be a general statistically stationary state in finite lattices, with a spectrum of Lyapunov exponents where the largest one grows roughly proportional to the logarithm of the nonlinearity index.

We would like to mention here also several aspects that deserve further investigations. Recently, the problem of heat transport in one-dimensional lattices has attracted a lot of attention [33]; here, the properties of strongly nonlinear lattices may differ from those possessing linear waves. Also a quantization of these lattices seems to be a nontrivial task, as there are no linear phonons to start with. Finally, the Anderson localization property of disordered lattices has been recently intensively discussed for nonlinear systems. For strongly nonlinear lattices the problem has to be attacked separately, as here one cannot rely on the spectral properties of a linear disordered system.

ACKNOWLEDGMENTS

We thank P. Rosenau and D. Shepelyansky for constant stimulating discussions. The work was supported by DFG via Grant No. PI-220/10 and via Collaborative Research Project 555 "Complex nonlinear processes."

[1] A focus issue on "The "Fermi-Pasta-Ulam" problem—the first 50 years," edited by D. K. Campbell, P. Rosenau, and G. Zaslavsky, Chaos **15**(1), 015101 (2005).
[2] S. Flach and C. R. Willis, Phys. Rep. **295**, 181 (1998).
[3] V. F. Nesterenko, J. Appl. Mech. Tech. Phys. **24**, 733 (1983).
[4] C. Coste, E. Falcon, and S. Fauve, Phys. Rev. E **56**, 6104 (1997).
[5] A. Chatterjee, Phys. Rev. E **59**, 5912 (1999).
[6] M. A. Porter, C. Daraio, E. B. Herbold, I. Szelengowicz, and P. G. Kevrekidis, Phys. Rev. E **77**, 015601(R) (2008).
[7] A. N. Lazaridi and V. F. Nesterenko, J. Appl. Mech. Tech. Phys. **26**, 405 (1985).
[8] S. L. Gavrilyuk and V. F. Nesterenko, J. Appl. Mech. Tech. Phys. **34**, 784 (1994).
[9] V. Nesterenko, *Dynamics of Heterogeneous Materials* (Springer, New York, 2001).
[10] P. Rosenau and J. M. Hyman, Phys. Rev. Lett. **70**, 564 (1993).
[11] P. Rosenau, Phys. Rev. Lett. **73**, 1737 (1994).

[12] R. S. Sinkovits and S. Sen, Phys. Rev. Lett. **74**, 2686 (1995).
[13] S. Sen and R. S. Sinkovits, Phys. Rev. E **54**, 6857 (1996).
[14] S. Sen, M. Manciu, and J. D. Wright, Phys. Rev. E **57**, 2386 (1998).
[15] M. Manciu, V. N. Tehan, and S. Sen, Chaos **10**, 658 (2000).
[16] M. Manciu, S. Sen, and A. J. Hurd, Phys. Rev. E **63**, 016614 (2000).
[17] S. Sen and M. Manciu, Phys. Rev. E **64**, 056605 (2001).
[18] E. Hascoët and E. J. Hinch, Phys. Rev. E **66**, 011307 (2002).
[19] A. Rosas and K. Lindenberg, Phys. Rev. E **68**, 041304 (2003).
[20] A. Rosas and K. Lindenberg, Phys. Rev. E **69**, 037601 (2004).
[21] S. Job, F. Melo, A. Sokolow, and S. Sen, Phys. Rev. Lett. **94**, 178002 (2005).
[22] S. Sen, J. Hong, J. Bang, E. Avalos, and R. Doney, Phys. Rep. **462**, 21 (2008).
[23] G. Friesecke and J. Wattis, Commun. Math. Phys. **161**, 391 (1994).
[24] R. S. MacKay, Phys. Lett. A **251**, 191 (1999).
[25] P. Rosenau, Phys. Lett. A **311**, 39 (2003).
[26] V. F. Nesterenko, J. Phys. IV **4**, C8–729 (1994).
[27] D. Treschev, Discrete Contin. Dyn. Syst. **11**, 867 (2004).
[28] V. I. Petviashvili, Sov. J. Plasma Phys. **2**, 257 (1976).
[29] V. I. Petviashvili, Physica D **3**, 329 (1981).
[30] *Handbook of Mathematical Functions*, Natl. Bur. Stand. Appl. Math. Ser. No. 55, edited by M. Abramowitz and I. A. Stegun (U.S. GPO, Washington, D.C., 1965).
[31] K. Ahnert and M. Abel, Comput. Phys. Commun. **177**, 764 (2007).
[32] S. Sen, K. Mohan, and J. Pfannes, Physica A **342**, 336 (2004).
[33] S. Lepri, R. Livi, and A. Politi, Phys. Rep. **377**, 1 (2003).